

PHASE ANGLE RATIO IMAGES OF COLOR INDEX $C(610/480 \text{ nm})$ OF WEST PORTION OF THE LUNAR NEARSIDE. S. Yu. Gerasimenko, V. G. Kaydash, Yu. G. Shkuratov, N. V. Opanasenko, Yu. I. Velikodsky, and V. V. Korokhin, Astronomical Institute of Kharkov V.N. Karazin National University, Sumskaya Street 35, Kharkov, 61022 Ukraine. gerasimenko@astron.kharkov.ua.

Introduction: Spectral observations of the Moon, including studies with recent lunar missions, e.g., [1], provide data on phase angle dependence of color indexes (ratios) in visible and NIR spectral range. Studies of such dependences are necessary for interpretation of lunar spectra. We map the color index phase ratios (CIPR) for west portion of the lunar nearside. We use telescope images acquired in the 2° - 95° range of phase angle α . At α from the range 2 - 50° , the color index $C_{R/B} = A(610 \text{ nm})/A(480 \text{ nm})$ of highlands grows with α faster than that for mare areas (A is albedo). The opposite effect is observed at larger α , 50° - 95° .

Retrieval the color index data: Lunar imaging campaign was organized in 2006 at the Maidanak observatory (Uzbekistan) [2,3]. Observations with the Kharkov 0.5-m reflector and Canon EOS 350D camera were carried out. The camera CMOS sensor is exploited using raw format imaging in three wide spectral bands ($\lambda_{\text{eff}} = 480$ (B), 540 (G), 610 nm (R)). The pixel readouts are calibrated to the numbers proportional to brightness of the lunar surface. In data processing we account for the electric zero, bias signal and the flat field. We improved the photometric accuracy of the data by coregistering and averaging images obtained during short time. All the images obtained at different solar illumination were transformed into common projection allowing their quantitative comparison.

Results of CIPR mapping: We apply the phase angle ratio method (e.g., [2]) to study the dependence of the color index on phase angles. We calculate the ratio of two $C_{R/B}$ images that are constructed for different α_1 and α_2 . Thus, $C_{R/B}$ variations are suppressed on the phase angle ratio image $\text{CIPR} = C_{R/B}(\alpha_1)/C_{R/B}(\alpha_2)$, $\alpha_1 < \alpha_2$, and only the difference of $C_{R/B}$ phase dependences should remain. We here do not use an absolute photometric calibration, i.e. our estimates of the CIPR behavior are relative.

We have investigated the $C_{R/B}$ phase angle trend for both west and east portions of the lunar nearside. Here we present results for the west nearside region that comprises Mare Humorum, southern Procellarum and surrounding south-western highlands. Figure 1 shows an image mosaic of the region in G filter. Figure 2 presents a $C_{R/B}$ image mosaic. Color variations over the image are about 13 %. Brighter tones correspond to higher $C_{R/B}$ values. The color-index map reveals differ-

ences between west and east parts of Mare Humorum. The “blue” mare region near the crater Flamsteed is also show up on the map.

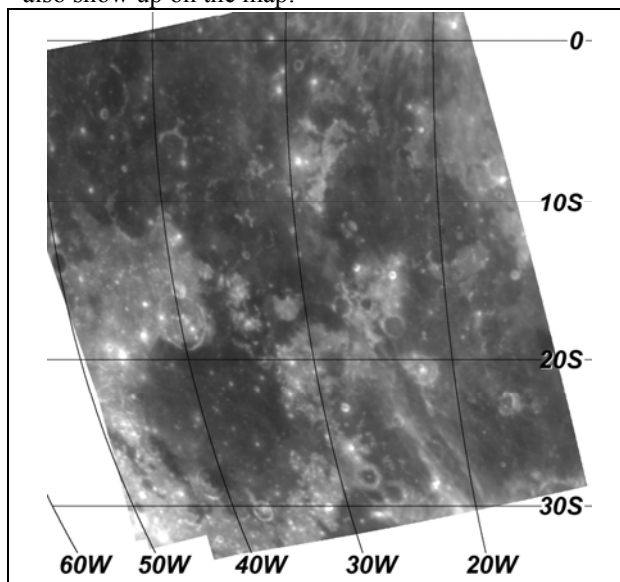


Figure 1. Brightness distribution (mosaic) in G filter over the southern Procellarum.

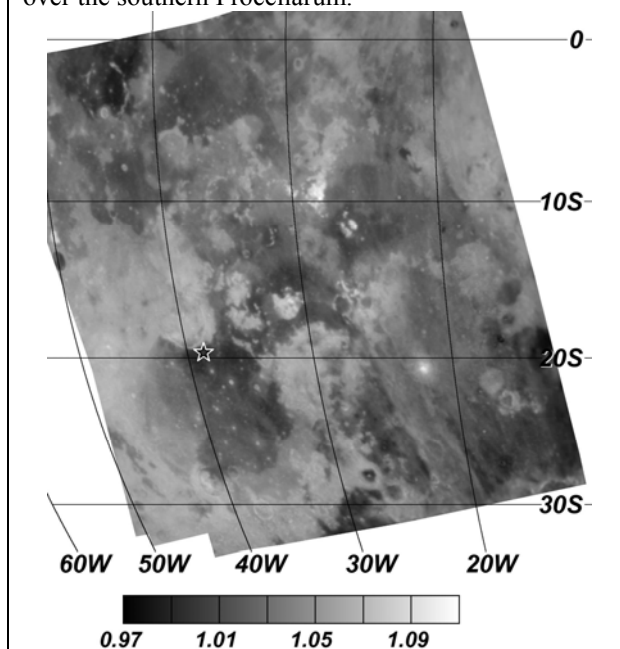


Figure 2. Color index $C_{R/B}$ distribution (mosaic). Star shows the site used for color-index normalization (MH-1A standard [4]).

We have constructed a series of CIPR images of the region at different combinations of α . We here show only two CIPR distributions: for small ($2^\circ/11^\circ$) (Fig. 3) and large ($57^\circ/96^\circ$) (Fig. 4) phase angle ranges. Analysis of the presented images reveals a relative excess of the CIPR ($2^\circ/11^\circ$) for mare regions over highlands, up to 2-3 %. Lowest values of the parameter are observed for the crater Gassendi and southern montes Rhiphaeus. In general, anticorrelation of the CIPR with albedo (cf. Fig. 1) is observed. We note that CIPR variations over bright young craters and ray systems are sufficiently suppressed. The CIPR ($57^\circ/96^\circ$) distribution (Fig. 4) shows well-observed direct correlation with albedo. The lowest value of the CIPR is found for small area in the south of Mare Humorum. The CIPR for highlands is $\sim 3\%$ higher than that for mare areas. Note that regions in east portion of the lunar nearside exhibit similar features of CIPR in the same α ranges.

Discussion: CIPR mapping reveals inverse correlation with albedo at small phase angles. At larger phase angles the weakening “mare/highland” contrast on the CIPR image is observed. In the range of $\alpha \sim 40^\circ$ - 50° the “mare/highland” contrast is disappeared. Finally, at $\alpha > 40^\circ$ - 50° the direct correlation of CIPR with albedo becomes distinguishable. The phase angle reddening, i.e. the growth of $C_{R/B}$ with α is explained by the progressive contribution of higher scattering orders to the total light flux reflected by the lunar regolith. The higher the albedo (hence higher $C_{R/B}$), the greater contribution of multiple scattering. Thus, for the surface with higher $C_{R/B}$ this contribution is greater, and, therefore, the phase dependence of the color index is more expressed. Darker mare soils should have more neutral $C_{R/B}(\alpha)$ behavior in comparison with the highland material. Changing of the slope of $C_{R/B}(\alpha)$ curve for the phase angles $\alpha > 40^\circ$ - 60° is connected with diminishing of multiple scattering at very large angles. This was shown in computer modeling of light scattering in particulate surfaces [5,6].

Conclusion: Using the Earth-based telescope lunar survey, we mapped phase ratios of color index $C_{R/B}$ in the α range 2° - 95° . We observed the following behavior of $C_{R/B}$: for highlands the value of $C_{R/B}$ increases with α faster, than that for maria. This behavior remains up to the $\alpha \approx 45^\circ$. Then, the $C_{R/B}$ dependence on α goes steeper for maria than that for highlands. Investigations of phase angle dependences of color indexes are important, if any accurate spectrophotometric calibration is necessary. Particularly, it concerns data recently obtained by the space lunar missions LRO (USA), Kaguya (Japan), and Chandrayaan-1 (India).

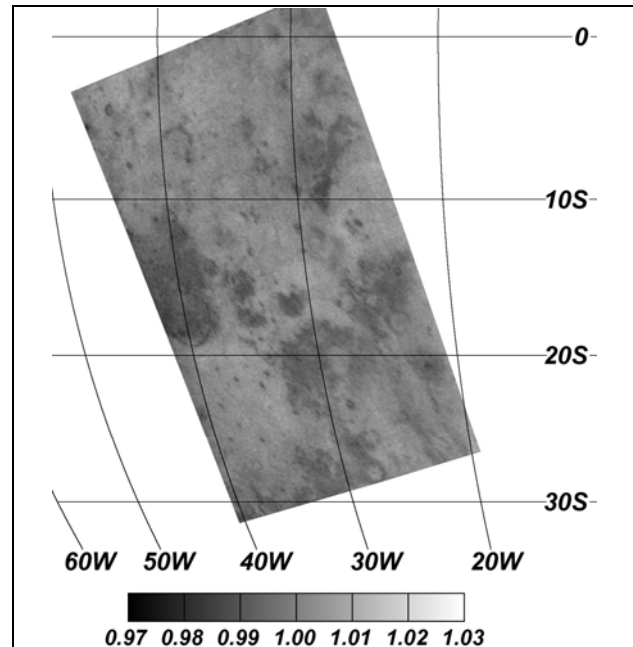


Figure 3. CIPR image $C_{R/B}(2^\circ)/C_{R/B}(11^\circ)$.

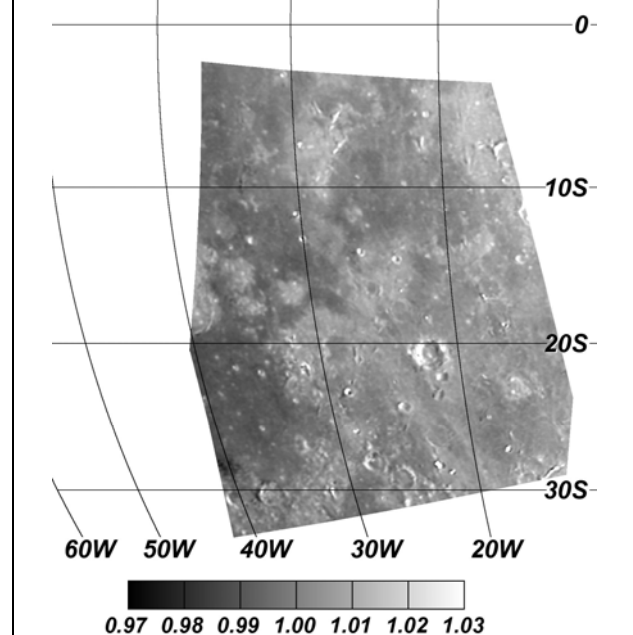


Figure 4. CIPR image $C_{R/B}(57^\circ)/C_{R/B}(96^\circ)$.

Acknowledgement: This study was supported by CRDF grant UKP2-2897-KK-07.

References: [1] Yokota Y. et al. (2009) *LPS XXXX*, Abstract #2525. [2] Kaydash V. G. et al. (2009) *Solar Sys. Res.*, 43, 89–99. [3] Opanasenko N. V. et al. (2009) *Solar Sys. Res.*, 43, 210–214. [4] Pieters C. M. (1986) *Reviews of Geophys.*, 24, No. 3, 557-578. [5] Stankevich D. et al. (2002) *JQSRT*, 76, No. 1, 1–16. [6] Stankevich D. and Shkuratov Yu. (2004) *JQSRT*, 87, No. 3-4, 289–296.